Aalborg Universitet

Semi-active feedforward control of a floating OWC point absorber for optimal power take-off

Sun, Tao; Nielsen, Søren R. K.

Published in:
IEEE Transactions on Sustainable Energy

DOI (link to publication from Publisher):
10.1109/TSTE.2019.2923279

Publication date:
2020

Document Version
Accepted author manuscript, peer reviewed version

Link to publication from Aalborg University

Citation for published version (APA):
Sun, T., & Nielsen, S. R. K. (2020). Semi-active feedforward control of a floating OWC point absorber for optimal power take-off. *IEEE Transactions on Sustainable Energy*, *11*(3), 1300-1308. Article 8737763. https://doi.org/10.1109/TSTE.2019.2923279

General rights
Copyright and moral rights for the publications made accessible in the public portal are retained by the authors and/or other copyright owners and it is a condition of accessing publications that users recognise and abide by the legal requirements associated with these rights.

- Users may download and print one copy of any publication from the public portal for the purpose of private study or research.
- You may not further distribute the material or use it for any profit-making activity or commercial gain
- You may freely distribute the URL identifying the publication in the public portal -

Take down policy
If you believe that this document breaches copyright please contact us at vbn@aub.aau.dk providing details, and we will remove access to the work immediately and investigate your claim.

Downloaded from vbn.aau.dk on: June 18, 2025

This article has been accepted for publication in a future issue of this journal, but has not been fully edited. Content may change prior to final publication. Citation information: DOI 10.1109/TSTE.2019.2923279, IEEE Transactions on Sustainable Energy

Semi-active feedforward control of a floating OWC point absorber for optimal power take-off

Tao Sun and Søren R.K. Nielsen

***Abstract*—The performance of a floating oscillating water column wave energy converter is depending on the variation of the pressure above atmospheric pressure in the pressure chamber above the water column. The pressure can be semi-actively controlled by the opening and closure of a valve between the pressure chamber and the generator. In the paper a control is suggested, where the closure time intervals of the valve are taken as a fixed fraction of the peak period of a given sea-state. The control relies on an estimation of the external wave loads, which in turn depend on the prediction of the future surface elevation in a given prediction interval, for which reason it is classified as a feedforward (open loop) control strategy. A Kalman-Bucy filter has been devised for the indicated prediction. The optimal fraction of time of the sub-optimal controller with a closed valve is determined by comparison with the performance of the optimal control obtained by nonlinear programming. For a given sea-state it is demonstrated that the reduced performance of the sub-optimal controller is primarily related to the estimation error of the wave loads.**

***Index Terms*—wave energy, oscillating water column, heave absorber, semi-active control, feedforward control**

I. Introduction

An Oscillating Water Column (OWC) wave energy converter (WEC) extracts energy by driving an oscillating water column which compresses or expands the air in a chamber not connected to the sea. The change of the internal energy of the air in the pressure chamber can next be transformed to electric energy via the generated air flow through a valve to the turbine. OWCs have been deployed as fixed structures at the shoreline or nearshore, or integrated in breakwaters and floating structures [1]. For the floating OWC device, the relative motion between the float and the internal free surface provides the air flow. One of the main advantages of floating OWC devices is that it is possible to widen the bandwidth of frequencies where the system performs well if the resonance peaks from the floater and water column are tuned to or close to the dominant wave frequency of the incoming wave [2]. In any case, in order to improve wave energy conversion an effective control strategy of the relative motion between the float and the surface of water column for a floating OWC devices or the motion of the surface of the water column for a fixed OWC device should be devised.

Reference [3] applied latching control for control of fixed OWC wave energy converter including the air turbine numerically. A valve, which switches rapidly between a closed and an open state, was applied to further improve the performance of the device. The closing of the valve causes a rapid increase of the pressure, which causes an increased power absorption at the succeeding reopening. The optimal control problem was derived by a variational approach with Hamiltonian formalism [4], and solved by the conditional gradient method [5]. It shows that phase-control of the oscillating water column is feasible for irregular waves and that energy-capture can be significantly increased by applying a flow-control in the power-conversion system. Reference [6] performed a numerical analysis of latching control of an OWC spar-buoy wave energy converter considering for regular waves. The compressibility of the air in the chamber plays an important role because it allows a relative motion between the floater and the internal free surface.

Further, in order to increase wave energy conversion, some studies for turbogenerator control of the OWC device have been performed. The aerodynamic design of the Wells turbine to the OWC performance was investigated by Brito-Melo et al., [7]. Garrido et al. presented a sliding-mode-control-based vector control scheme to improve the lacks of accuracy and robustness of parameters for PI controller [8]. A control scheme including a rotational speed control and an airflow control has been introduced to improve the wave energy conversion [9]. Flow behaviour between the air chamber and the turbine was investigated through CFD simulation by El Marjani et al., [10]. In the present paper, merely a Wells turbine is considered.

Generally, in order to analyze the interaction between the floater and the OWC, there are two different approaches, known as the piston model [11] and the uniform pressure distribution model [12], respectively. The piston model presumes that the vertical particle motion of the water column is constrained to move with the same displacement under the assumption of limited pressure chamber dimensions compared to the incident wavelengths [2], [13]. In the uniform pressure distribution model, the governing equations are expressed in terms of the dynamic air pressure on the OWC internal free surface and flow rate displace by the OWC surface motion, rather than forces and velocities as in the modelling of oscillating body converters. Further, for the piston model the interaction between waves and the WEC can be analysed by using the wave-structure interaction theory [11], [14] for a two-body coupling system. Therefore, the piston model is introduced to calculate the hydrodynamic parameters for the floating OWC system.

The paper presents a sub-optimal solution for the control of a floating OWC heave point absorber. Given the closure intervals of the valve are taken as a fixed fraction of the peak period of a given sea-state, the semi-active control of the opening and closure of a valve will be considered. Then,

The authors Tao Sun and Søren R.K. Nielsen are with the Department of Civil Engineering (e-mail: tsu@civil.aau.dk; srkn@civil.aau.dk).

Manuscript received XX XX, 2019; revised XX XX, 2019.

1949-3029 (c) 2019 IEEE. Personal use is permitted, but republication/redistribution requires IEEE permission. See http://www.ieee.org/publications_standards/publications/rights/index.html for more information.

This article has been accepted for publication in a future issue of this journal, but has not been fully edited. Content may change prior to final publication. Citation information: DOI 10.1109/TSTE.2019.2923279, IEEE Transactions on Sustainable Energy

the wave load vector, the input to the system, needs to be estimated. Finally, a numerical example is provided to investigate the performance of the suggested control algorithm.

II. Methodology

A. Equation of motion of the floating OWC device

When the internal water surface moves up, or the device structure moves down, the volume of the pressure chamber becomes smaller, which creates an increased pressure in the pressure chamber. The increased chamber pressure drives the air out of the pressure chamber, and at the same time pushes the device structure upward and the internal water surface downward, so that the air volume is enlarged.

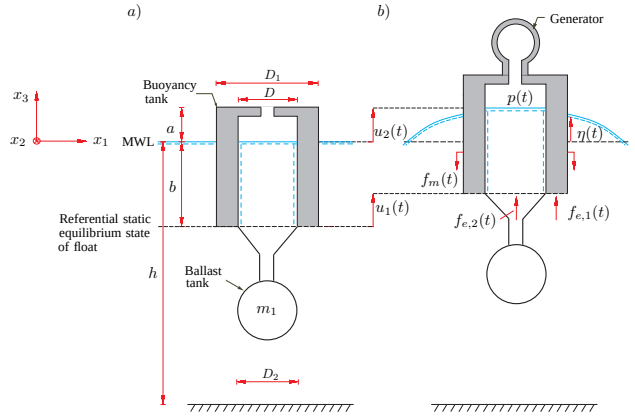

Fig. 1: Loads on floating OWC device. a) Static equilibrium state. b) Dynamic state.

Fig. 1a shows the floating OWC device in the static equilibrium state, where a and b indicates the parts of the float above and below the mean water level MWL. a is the height of the pressure chamber, and b is the submerged part of the pressure chamber. h specifies the water depth. The outer diameters of the buoyancy tank and ballast tank are D_1 and D_2, and D is the diameter of the water column. m_1 is the structural mass including the ballast.

The motion of the point absorber is referred to an inertial (x_1, x_2, x_3)-coordinate system with the (x_1, x_2)-plane positioned in the MWL-plane, and the x_3-axis orientated in the upwards direction. The origin of the coordinate system is placed at the centerline of the point absorber. The surface elevation $\eta(x_\beta, t)$ is considered positive in the x_3-direction. Index notation of two-dimensional vectorial quantities is applied with Greek indices ranging over $\alpha, \beta = 1, 2$ and Latin indices ranging over $k = 1, 2, 3$, respectively. The summation convention is abandoned by means of parentheses around dummy indices, i.e. $a_\alpha\, b_\alpha = a_1 b_1 + a_2 b_2$, whereas $a_{(\alpha)} b_{(\alpha)}$ merely indicates the product of a_α and b_α.

The water flow is considered incompressible, irrotational and non-viscous, and linear (Airy) wave theory is assumed. ρ_w signifies the mass density of the water. $p(x_k, t)$ signifies the thermodynamic pressure of the air in the pressure chamber above the atmospheric pressure p_0. The pressure is assumed to be constant throughout the pressure chamber, so $p(x_k, t) \simeq p(t)$.

The surface elevation $\eta(x_\beta, t)$ inside the pressure chamber is dominated by the mean surface elevation $u_2(t)$ of the water column from the MWL. Hence, the following approximation applies:

$$\eta(x_\beta, t) \simeq u_2(t) \tag{1}$$

Equation (1) is known as the piston approximation. Since the water column is assumed to be infinite rigid, the constraint can be imposed at any position along the length b at the water column, if the mass of the water column above the constraint is added as a point mass m_2.

Let $u_1(t)$ be the vertical displacement of the float in the x_3-direction. For the float, the pressure produces a force $p(t)A$ on the system in the direction of the degree of freedom $u_1(t)$, and a force $-p(t)A$ on the water column in the direction of the degree of freedom $u_2(t)$, where $A = \frac{\pi}{4} D^2$ indicates the surface area of the water column. Further, the vertical components of the dynamic restoring force from the mooring system are given by the linear stiffness relation $f_m(t) = k_m\, u_1(t)$, where km is the combined stiffness coefficient from all cables. Due to the piston model, the following vectorial Cummings equation applies:

$$\left.\begin{aligned} &\mathbf{M}\,\ddot{\mathbf{u}}(t) + \mathbf{f}_r(t) + \mathbf{r}\big(\mathbf{u}(t)\big) = \mathbf{f}_e(t) - \mathbf{f}_c(t)\ ,\ t \in]t_0, t_1] \\ &\mathbf{u}(t_0) = \mathbf{u}_0\ ,\ \dot{\mathbf{u}}(t_0) = \dot{\mathbf{u}}_0 \end{aligned}\right\} \tag{2}$$

where

$$\left.\begin{aligned} \mathbf{u}_0 &= \begin{bmatrix} u_{1,0}(t) \\ u_{2,0}(t) \end{bmatrix} \quad , \quad \dot{\mathbf{u}}_0 = \begin{bmatrix} \dot{u}_{1,0}(t) \\ \dot{u}_{2,0}(t) \end{bmatrix} \\ \mathbf{u}(t) &= \begin{bmatrix} u_1(t) \\ u_2(t) \end{bmatrix} \quad , \quad \mathbf{f}_c(t) = \mathbf{a}\, p(t) \quad , \quad \mathbf{a} = \begin{bmatrix} -1 \\ 1 \end{bmatrix} A \\ \mathbf{f}_e(t) &= \begin{bmatrix} f_{e,1}(t) \\ f_{e,2}(t) \end{bmatrix} \quad , \quad \mathbf{r}\big(\mathbf{u}(t)\big) = \begin{bmatrix} (k_m + \rho_w\, g\, A_1)\, u_1(t) \\ \rho_w\, g\, A\, u_2(t) \end{bmatrix} \\ \mathbf{M} &= \begin{bmatrix} m_1 + m_{11}(\infty) & m_{12}(\infty) \\ m_{21}(\infty) & m_2 + m_{22}(\infty) \end{bmatrix} \end{aligned}\right\} \tag{3}$$

t_0 is the initial time, and t_1 the terminal time of the control horizon. $\mathbf{u}_0$ and $\dot{\mathbf{u}}_0$ signify the initial value vectors of the system at the initial time t_0. $A_1 = \frac{\pi}{4}(D_1^2 - D^2)$ is the sectional area of the float surrounding the pressure chamber.

$\mathbf{f}_e(t)$ is a vector storing the external wave load vector and $\mathbf{r}\big(\mathbf{u}(t)\big)$ specifies the restoring force from buoyancy and the mooring system. ρ_w indicates the mass density of the water and g is the acceleration of gravity. $\mathbf{M}$ signifies the mass matrix. The components $m_{\alpha\beta}(\infty)$ indicate the added mass matrix of the water outside the float and below the piston at infinite frequency. $\mathbf{f}_r(t)$ represents the radiation damping of the system given as:

$$\mathbf{f}_r(t) = \int_{t_0}^{t} \mathbf{h}_r(t - \tau)\, \dot{\mathbf{u}}(\tau)\, d\tau \tag{4}$$

The related frequency response matrix is given by the Fourier transform:

$$\mathbf{H}_r(\omega) = \int_{-\infty}^{\infty} \mathrm{e}^{-i\omega t}\, \mathbf{h}_r(t)\, dt = \int_{0}^{\infty} \mathrm{e}^{-i\omega t}\, \mathbf{h}_r(t)\, dt \tag{5}$$

where i indicates the complex unit. In the last statement it has been used that $\mathbf{h}_r(t)$ is causal, i.e. $\mathbf{h}_r(t) = \mathbf{0}$, $t < 0$, which makes a rational approximation to $\mathbf{f}_r(t)$ possible.

1949-3029 (c) 2019 IEEE. Personal use is permitted, but republication/redistribution requires IEEE permission. See http://www.ieee.org/publications_standards/publications/rights/index.html for more information.

This article has been accepted for publication in a future issue of this journal, but has not been fully edited. Content may change prior to final publication. Citation information: DOI 10.1109/TSTE.2019.2923279, IEEE Transactions on Sustainable Energy

The external wave load vector may be represented by the following convolution integral of the surface elevation $\eta(t)$:

$$\mathbf{f}_e(t) = \int_{-\infty}^{\infty} \mathbf{h}_e(t-\tau)\,\eta(\tau)\,d\tau \qquad (6)$$

where $\mathbf{h}_e(t)$ indicates a non-causal impulse response vector because $\mathbf{h}_e(t) \neq \mathbf{0}, t < 0$. Due to the non-causality of $\mathbf{h}_e(t)$, the prediction of the surface elevation $\eta(\tau), \tau > t$ is necessary in order to calculate the wave loads at the time t.

The hydrodynamic parameters $m_{\alpha\beta}$, $\mathbf{h}_r(t)$, $\mathbf{h}_e(t)$ are computed based on the boundary element program WAMIT [15]. Fig. 2 shows the submerged geometry discretization for the floating OWC device. The kinematic constraint has been specified at the bottom of the water column as marked in blue. Correspondingly, $m_2 = \rho_w\, A\, b$.

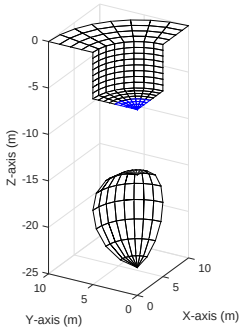

Fig. 2: The submerged geometry discretization for the floating OWC device.

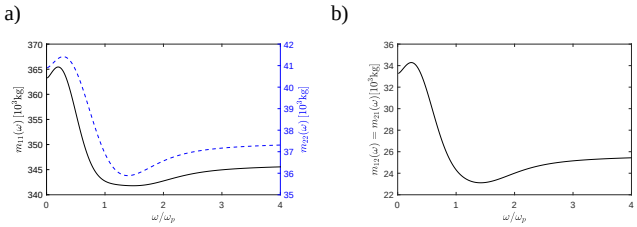

Fig. 3: Hydrodynamic added mass matrix. ——: The float. - - - : The OWC.

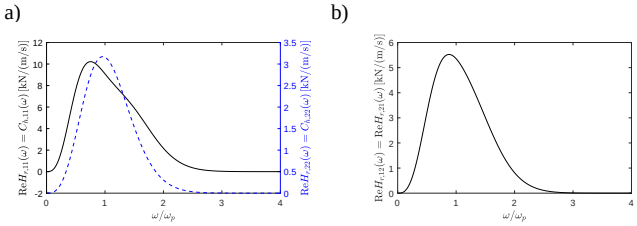

Fig. 4: Imaginary part of the frequency response matrix for the radiation force vector. ——: The float. - - - : The OWC.

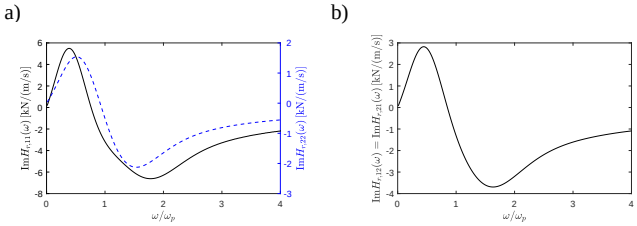

Fig. 5: Real part of the frequency response matrix for the radiation force vector. ——: The float. - - - : The OWC.

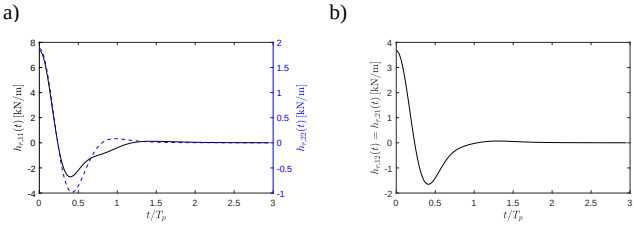

Fig. 6: Impulse response matrix for the radiation force vector. ——: The float. - - - : The OWC.

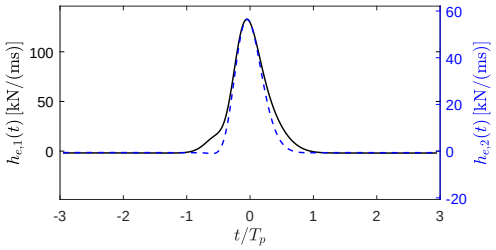

Fig. 7: Impulse response vector for the excitation force vector. ——: The float. - - - : The OWC.

Fig. 3 shows the hydrodynamic added mass for the float and the OWC. Figs. 3-7 refer to the absorber shown in Fig. 1 with the parameter values given in Table I in the numerical example. The angular frequency ω has been normalized with respect to the peak angular frequency $\omega_p = \frac{2\pi}{T_p}$, where T_p is the peak period of the considered sea-state.

The real and imaginary parts of the related frequency response matrix for the radiation force are shown in Figs. 4 and 5. Merely the function values for positive angular frequency, given that $\mathrm{Re}\big(H_{r,\alpha\beta}(\omega)\big)$ is an even function and $\mathrm{Im}\big(H_{r,\alpha\beta}(\omega)\big)$ is an odd function of ω.

The impulse response matrices for the radiation force and wave load vectors are shown in Figs. 6 and 7. The impulse response matrix $\mathbf{h}_r(t)$ is symmetric, i.e., $\mathbf{h}_r(t) = \mathbf{h}_r^T(t)$ as indicated in Fig. 6b. In turn this means that the frequency response matrix $\mathbf{H}_r(\omega)$ and the related added mass matrix $\mathbf{m} = \frac{1}{\omega}\mathrm{Im}(\mathbf{H}_r(\omega))$ become symmetric as well. As seen, $h_{e\eta,\alpha}(t) \simeq 0$ for $|t| > T_p$. Hence, surface elevations beyond one peak wave period ahead will not affect the present wave load vector $\mathbf{f}_e(t)$.

B. Thermodynamics of the air

The air is considered an adiabatic, isentropic ideal gas. Then, the pressure is given by the constitutive equation [16]:

$$\frac{p(t)+p_0}{p_0} = \left(\frac{\rho(t)}{\rho_0}\right)^{\gamma} \quad , \quad \gamma = \frac{c_p}{c_v} \simeq 1.4 \qquad (7)$$

where $\rho(t)$ indicates the time-varying mass density of air, ρ_0 is the referential value at atmospheric pressure, and c_p and c_v indicate the specific heat at constant pressure and constant volume.

p_0 turns out to be significantly larger than even extreme values of $p(t)$ in a practical OWC device. Hence, equation (7)

1949-3029 (c) 2019 IEEE. Personal use is permitted, but republication/redistribution requires IEEE permission. See http://www.ieee.org/publications_standards/publications/rights/index.html for more information.

This article has been accepted for publication in a future issue of this journal, but has not been fully edited. Content may change prior to final publication. Citation information: DOI 10.1109/TSTE.2019.2923279, IEEE Transactions on Sustainable Energy

can be linearised to provide the following approximation for $\rho(t)$:

$$\rho(t) \simeq \rho_0 \left(1 + \frac{p(t)}{\gamma\, p_0}\right) \tag{8}$$

The pressure variation $p(t)$ in the air chamber is related to the volume flow rate of air through the turbine (positive for outward flow). The pressurized air is driven out in exhalation, while in inhalation, the atmosphere air with the density ρ_0 is inhaled. Thus, the air volume flow rate during exhalation and inhalation should be considered different due to the different mass densities corresponding to:

$$Q(t) = \begin{cases} -\dfrac{1}{\rho(t)} \dfrac{d\big(\rho(t)\, V(t)\big)}{dt} & , \quad p(t) \geq 0 \\ -\dfrac{1}{\rho_0} \dfrac{d\big(\rho(t)\, V(t)\big)}{dt} & , \quad p(t) < 0 \end{cases} \tag{9}$$

where $V(t) = V_0 + A\,\big(u_1(t) - u_2(t)\big)$ is the volume of the air chamber. $V_0 = A\,a$ is the initial volume of the air chamber. Then, $\dot{V}(t)$ can be written as:

$$\dot{V}(t) \;=\; A\,\big(\dot{u}_1(t) - \dot{u}_2(t)\big) \tag{10}$$

Differentiation of (8) provides:

$$\dot{\rho}(t) \;=\; \frac{\rho_0}{\gamma\, p_0}\, \dot{p}(t) \tag{11}$$

In the following a Wells turbine is considered, for which the mass flow is given as [7]:

$$Q(t) \;=\; k\, \beta(t)\, p(t) \tag{12}$$

where k is a constant which represents the damping of the turbine. $\beta(t)$ represents the proportional opening of the valve and is constrained to satisfy $0 \leq \beta(t) \leq 1$.

Further, in order to avoid the stalling behavior of the Wells turbine when the airflow exceeds a certain value, greatly decreasing its efficiency, the airflow speed through the turbine must be limited, which can be carried out by the air-valve control, which is widely used in OWC systems [17], [18]. Alternatively, control of the rational speed can be applied to avoid the stalling behavior [19].

Combining Eqs. (9), (10), (11) and (12), the following differential equation is obtained, which relates the air pressure variation $p(t)$ to the relative velocity of the inner free surface and the float.

$$\begin{cases} \dot{p}(t) V(t) + (\gamma p_0 + p(t)) \Big(\dot{V}(t) + k\, \beta(t)\, p(t)\Big) \;=\; 0,\; p(t) \geq 0 \\ \dfrac{V(t)}{\gamma p_0} \dot{p}(t) + \left(1 + \dfrac{p(t)}{\gamma p_0}\right) \dot{V}(t) + k\, \beta(t)\, p(t) \;=\; 0,\; p(t) < 0 \end{cases} \tag{13}$$

For the turbine, the instantaneous absorbed power can be expressed as [20]:

$$P(t) \;=\; Q(t)\, p(t) \tag{14}$$

Insertion of (12) in (14) provides the following relation for the instantaneous power take-off:

$$P(t) \;=\; k\, \beta(t)\, p^2(t) \tag{15}$$

The dynamic of the system is given by (2) in combination to (13), corresponding to:

$$\left.\begin{array}{l} \mathbf{M}\, \ddot{\mathbf{u}}(t) \,+\, \mathbf{f}_r(t) \,+\, \mathbf{r}\big(\mathbf{u}(t)\big) \;=\; \mathbf{f}_e(t) \,-\, \mathbf{f}_c(t)\;,\; t \in]t_0, t_1] \\ \left.\begin{array}{r} \dot{p}(t) + \dfrac{\gamma p_0 + p(t)}{V(t)} \Big(\dot{V}(t) + k\, \beta(t)\, p(t)\Big) \;=\; 0,\; p(t) \geq 0 \\ \dot{p}(t) + \big(\gamma p_0 + p(t)\big) \dfrac{\dot{V}(t)}{V(t)} + \dfrac{\gamma\, p_0\, k\, \beta(t)\, p(t)}{V(t)} \;=\; 0,\; p(t) < 0 \end{array}\right\} \\ \mathbf{u}(t_0) \;=\; \mathbf{u}_0\;,\; \dot{\mathbf{u}}(t_0) \;=\; \dot{\mathbf{u}}_0\;,\; p(t_0) = 0 \end{array}\right\} \tag{16}$$

The semi-active control of the system is related to the time variation of the function $\beta(t)$. The optimal control is the trajectory of $\beta(t)$, which optimizes the absorbed energy in the interval $[t_0, t_1]$ given as:

$$E \;=\; \int_{t_0}^{t_1} P(\tau)\, d\tau \;=\; \int_{t_0}^{t_1} k\, \beta(\tau)\, p^2(\tau)\, d\tau \tag{17}$$

C. Rational approximation to radiation force vector

In the following, an approximate finite dimensional state vector representation of $\mathbf{f}_r(t)$ will be introduced. It should be noticed that the indicated state vector representation will be used in the numerical time integration of (16), and the nonlinear programming solution for the optimal power take-off.

Then, each component $H_{r,\alpha\beta}(\omega) = H_{r,\beta\alpha}(\omega)$ of the frequency response matrix $\mathbf{H}_r(\omega)$ defined by (5) are replaced by a rational approximation $\tilde{H}_{r,\alpha\beta}(s)$ of the order (l, m) given as [21]:

$$\tilde{H}_{r,\alpha\beta}(s) \;=\; \frac{P_{(\alpha)(\beta)}(s)}{Q_{(\alpha)(\beta)}(s)} \quad , \quad s = i\omega \tag{18}$$

where

$$\left.\begin{array}{l} P_{\alpha\beta}(s) \;=\; p_{0,\alpha\beta} s^l + p_{1,\alpha\beta} s^{l-1} \;+ \cdots + p_{l-1,\alpha\beta} s \;+ p_{l,\alpha\beta} \\ Q_{\alpha\beta}(s) \;=\; s^m \qquad + q_{1,\alpha\beta} s^{m-1} + \cdots + q_{m-1,\alpha\beta} s + q_{m,\alpha\beta} \end{array}\right\} \tag{19}$$

The parameters $p_{0,\alpha\beta}, p_{1,\alpha\beta}, \ldots, p_{l-1,\alpha\beta}, p_{l,\alpha\beta}$ and $q_{1,\alpha\beta}, \ldots, q_{m-1,\alpha\beta}, q_{m,\alpha\beta}$ are all real. The order (l, m) of the filters may be chosen freely with the only restrictions that $l < m$, and that all poles of $Q_{\alpha\beta}(s)$ must have negative real parts in order to ensure stability and causality.

The component $f_{r,\alpha\beta}(t)$ indicates the contribution to the component $f_{r,\alpha}(t)$ of $\mathbf{f}_r(t)$, when the system is driven by component $\dot{u}_\beta(t)$ of $\dot{\mathbf{u}}(t)$ alone. Further, the relationship between $\mathbf{f}_r(t), f_{r,\alpha}(t), f_{r,\alpha\beta}(t)$ can be expressed as:

$$\mathbf{f}_r(t) \;=\; \begin{bmatrix} f_{r,1}(t) \\ f_{r,2}(t) \end{bmatrix} \;=\; \begin{bmatrix} f_{r,11}(t) \,+\, f_{r,12}(t) \\ f_{r,21}(t) \,+\, f_{r,22}(t) \end{bmatrix} \tag{20}$$

Then, $f_{r,\alpha\beta}(t)$ can be obtained as output of the following filter equations, given on the matrix form:

$$\left.\begin{array}{l} f_{r,\alpha\beta}(t) \;=\; \mathbf{p}_{r,(\alpha)(\beta)}\, \mathbf{z}_{r,(\alpha)(\beta)}(t) \\ \dfrac{d}{dt} \mathbf{z}_{r,\alpha\beta}(t) \;=\; \mathbf{A}_{r,(\alpha)(\beta)}\, \mathbf{z}_{r,(\alpha)(\beta)}(t) + \mathbf{b}_{r,(\alpha)(\beta)} \dot{u}_{(\beta)}(t),\; t \in [t_0, \infty[\end{array}\right\} \tag{21}$$

1949-3029 (c) 2019 IEEE. Personal use is permitted, but republication/redistribution requires IEEE permission. See http://www.ieee.org/publications_standards/publications/rights/index.html for more information.

This article has been accepted for publication in a future issue of this journal, but has not been fully edited. Content may change prior to final publication. Citation information: DOI 10.1109/TSTE.2019.2923279, IEEE Transactions on Sustainable Energy

where

$$\mathbf{z}_{r,\alpha\beta}(t) = \begin{bmatrix} y_{\alpha\beta}(t) \\ \frac{d}{dt}y_{\alpha\beta}(t) \\ \frac{d^2}{dt^2}y_{\alpha\beta}(t) \\ \vdots \\ \frac{d^{m-1}}{dt^{m-1}}y_{\alpha\beta}(t) \end{bmatrix}, \quad \mathbf{b}_{r,\alpha\beta} = \begin{bmatrix} 0 \\ 0 \\ 0 \\ \vdots \\ 1 \end{bmatrix} \tag{22}$$

$$\mathbf{A}_{r,\alpha\beta} = \begin{bmatrix} 0 & 1 & 0 & \cdots & 0 & 0 \\ 0 & 0 & 1 & \cdots & 0 & 0 \\ \vdots & \vdots & \vdots & \ddots & \vdots & \vdots \\ 0 & 0 & 0 & \cdots & 0 & 1 \\ -q_{m,\alpha\beta} & -q_{m-1,\alpha\beta} & -q_{m-2,\alpha\beta} & \cdots & -q_{2,\alpha\beta} & -q_{1,\alpha\beta} \end{bmatrix} \tag{23}$$

$$\mathbf{p}_{r,\alpha\beta} = \begin{bmatrix} p_{l,\alpha\beta} & p_{l-1,\alpha\beta} & \cdots & p_{1,\alpha\beta} & p_{0,\alpha\beta} & 0 & \cdots & 0 \end{bmatrix} \tag{24}$$

Finally, equation (21) can be written on the matrix form:

$$\left.\begin{aligned} \frac{d}{dt}\mathbf{z}_r(t) &= \mathbf{A}_r\,\mathbf{z}_r(t) + \mathbf{B}_r\,\dot{\mathbf{u}}(t) \\ \mathbf{f}_r(t) &= \mathbf{P}_r\,\mathbf{z}_r(t) \end{aligned}\right\} \tag{25}$$

where

$$\left.\begin{aligned} \mathbf{A}_r &= \begin{bmatrix} \mathbf{A}_{r,11} & \mathbf{0} & \mathbf{0} & \mathbf{0} \\ \mathbf{0} & \mathbf{A}_{r,12} & \mathbf{0} & \mathbf{0} \\ \mathbf{0} & \mathbf{0} & \mathbf{A}_{r,21} & \mathbf{0} \\ \mathbf{0} & \mathbf{0} & \mathbf{0} & \mathbf{A}_{r,22} \end{bmatrix}, \mathbf{B}_r = \begin{bmatrix} \mathbf{b}_{r,11} & \mathbf{0} \\ \mathbf{0} & \mathbf{b}_{r,12} \\ \mathbf{b}_{r,21} & \mathbf{0} \\ \mathbf{0} & \mathbf{b}_{r,22} \end{bmatrix} \\ \mathbf{P}_r &= \begin{bmatrix} \mathbf{p}_{r,11}\mathbf{p}_{r,12} & \mathbf{0} & \mathbf{0} \\ \mathbf{0} & \mathbf{0} & \mathbf{p}_{r,21}\mathbf{p}_{r,22} \end{bmatrix}, \mathbf{z}_r(t) = \begin{bmatrix} \mathbf{z}_{r,11}(t) \\ \mathbf{z}_{r,12}(t) \\ \mathbf{z}_{r,21}(t) \\ \mathbf{z}_{r,22}(t) \end{bmatrix} \end{aligned}\right\} \tag{26}$$

Further, the differential equation (25) should be solved with the initial value $\mathbf{z}_r(t_0) = \mathbf{0}$. Notice that $\mathbf{A}_{r,12} = \mathbf{A}_{r,21}$, $\mathbf{b}_{r,12} = \mathbf{b}_{r,21}$ and $\mathbf{p}_{r,12} = \mathbf{p}_{r,21}$ due to the symmetry of $\tilde{\mathbf{H}}_r(\omega)$.

Figs. 8 - 10 show the rational approximation $\tilde{H}_{r,\alpha\beta}(\omega)$ of order $(l,m) = (3,4)$. As seen, a good agreement is obtained to the target frequency response functions $H_{r,\alpha\beta}(\omega)$. Further, time has been normalized with respect to the peak period T_p in the auto-spectrum density function for the surface elevation $\eta(t)$ given by (29), and the angular frequency with respect to $\omega_p = \frac{2\pi}{T_p}$. $T_p = 6.77$s was used, cf. Table I.

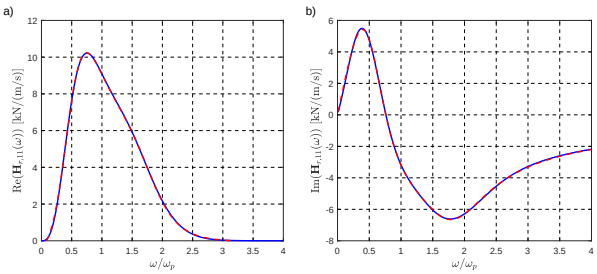

Fig. 8: Rational approximation of order $(m,n) = (3,4)$ to $H_{r,11}(\omega)$. a) $\mathrm{Re}\big(H_{r,11}(\omega)\big)$. c) $\mathrm{Im}\big(H_{r,11}(\omega)\big)$. ——: Numerical determined target. - - - : Rational approximation.

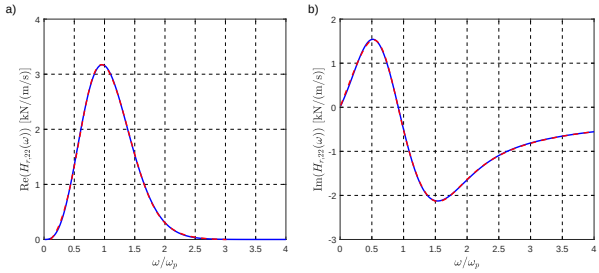

Fig. 9: Rational approximation of order $(m,n) = (3,4)$ to $H_{r,22}(\omega)$. a) $\mathrm{Re}\big(H_{r,22}(\omega)\big)$. c) $\mathrm{Im}\big(H_{r,22}(\omega)\big)$. ——: Numerical determined target. - - - : Rational approximation.

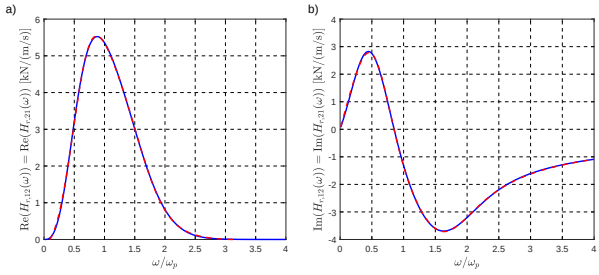

Fig. 10: Rational approximation of order $(m,n) = (3,4)$ to $H_{r,12}(\omega)$. a) $\mathrm{Re}\big(H_{r,12}(\omega)\big)$. c) $\mathrm{Im}\big(H_{r,11}(\omega)\big)$. ——: Numerical determined target. - - - : Rational approximation .

III. Nonlinear Programming Solution of the Optimal Control Problem

Based on Eqs. (15), (16) and (25), the optimal control problem subject to the following state equation can be expressed as:

$$\left.\begin{aligned} &\max J[p,\beta] = \int_{t_0}^{t_1} k\,\beta(\tau)\,p^2(\tau)d\tau \\ &\text{s.t.} \\ &\dot{\mathbf{z}}(t) = \begin{bmatrix} \dot{\mathbf{u}}(t) \\ \mathbf{M}^{-1}\Big(-\mathbf{P}_r\,\mathbf{z}_r(t) - \mathbf{r}\big(\mathbf{u}(t)\big) + \big(\mathbf{f}_e(t) - \mathbf{a}\,p(t)\big)\Big) \\ \mathbf{A}_r\,\mathbf{z}_r(t) + \mathbf{B}_r\,\dot{\mathbf{u}}(t) \\ \left.\begin{aligned} -\frac{\gamma p_0 + p(t)}{V(t)}\Big(\dot{V}(t) + k\,\beta(t)\,p(t)\Big)\,, & \; p(t) \geq 0 \\ -\big(\gamma p_0 + p(t)\big)\frac{\dot{V}(t)}{V(t)} - \frac{\gamma\,p_0\,k\,\beta(t)\,p(t)}{V(t)}\,, & \; p(t) < 0 \end{aligned}\right\} \end{bmatrix} \\ &0 \leq \beta(t) \leq 1 \end{aligned}\right\} \tag{27}$$

where

$$\mathbf{z}(t) = \begin{bmatrix} \mathbf{u}(t)^T & \dot{\mathbf{u}}(t)^T & \mathbf{z}_r(t)^T & p(t) \end{bmatrix}^T \tag{28}$$

The surface elevation $\eta(t)$ can be generated from the double-sided JONSWAP spectrum defined by [22]:

$$S_{\eta\eta}(\omega) = \delta\,\frac{H_s^2}{\omega_p}\,\psi^{\,\varepsilon}\left(\frac{|\omega|}{\omega_p}\right)^{-5}\exp\left(-\frac{5}{4}\left(\frac{\omega}{\omega_p}\right)^{-4}\right) \tag{29}$$

1949-3029 (c) 2019 IEEE. Personal use is permitted, but republication/redistribution requires IEEE permission. See http://www.ieee.org/publications_standards/publications/rights/index.html for more information.

This article has been accepted for publication in a future issue of this journal, but has not been fully edited. Content may change prior to final publication. Citation information: DOI 10.1109/TSTE.2019.2923279, IEEE Transactions on Sustainable Energy

where

$$\left.\begin{aligned} \delta &= \frac{0.0312}{0.230 + 0.0336\,\psi - \frac{0.185}{1.9+\psi}} \\ \varepsilon &= \exp\left(-\frac{1}{2}\left(\frac{|\omega| - \omega_p}{\sigma\,\omega_p}\right)^2\right) \\ \sigma &= \begin{cases} 0.07 & , \quad |\omega| \le \omega_p \\ 0.09 & , \quad |\omega| > \omega_p \end{cases} \end{aligned}\right\} \tag{30}$$

H_s is the significant wave height, and ψ is the peak enhancement parameter, which controls the bandwidth of the spectrum.

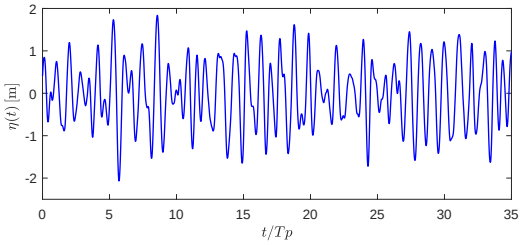

Fig. 11: Surface elevation process.

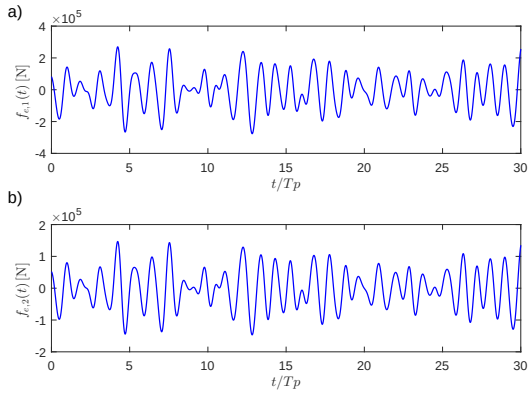

Fig. 12: Components of the wave load vector. a) The float. b) The OWC.

Fig. 11 shows a time series of $\eta(t)$ generated from the double-sided auto spectral density function in (29) with the parameters $T_p = 6.77\text{s}, \text{H}_\text{s} = 2.5\text{m}, \gamma = 3.3$. This and equivalent time series will be used in the bench-marking of the below suggested sub-optimal control strategy. Fig. 12 shows the time series of the related wave load components $f_{e,1}(t)$ and $f_{e,2}(t)$ on the float and the OWC as calculated by (6). The indicated time series will be used as a reference in the validation of the estimation problem described in Section 4.

The optimization problem in (27) can be solved by nonlinear programming [23], as a benchmark for the validation of the subsequent suggested control. Fig. 13 shows the trajectories of $\mathbf{u}(t)$, $\dot{\mathbf{u}}(t)$ and $\ddot{\mathbf{u}}(t)$ for the float and the OWC at optimal control, using the time series for the wave load given in Fig. 12. Further, the relative displacement $u_2(t) - u_1(t)$ is shown in Fig. 13a, which is determining the pressure in the pressure chamber.

Fig. 14 shows the related time series of $p(t)$ and $\beta(t)$ at optimal control indicated with a blue signature. $[t_1, t_3]$ and

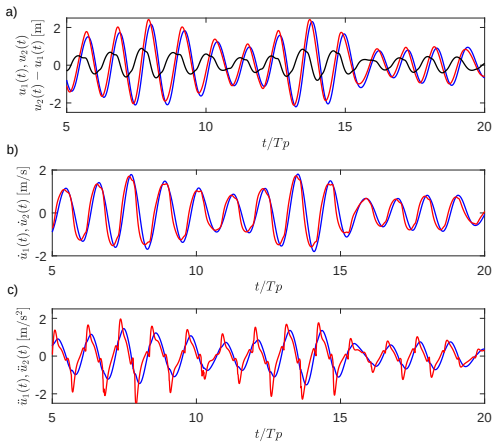

Fig. 13: Time series of trajectories at optimal control. ——: $u_1(t), \dot{u}_1(t), \ddot{u}_1(t)$. ——: $u_2(t), \dot{u}_2(t), \ddot{u}_2(t)$. ——: $u_2(t) - u_1(t)$.

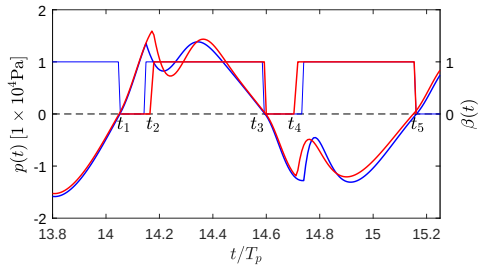

Fig. 14: $p(t)$ and $\beta(t)$ at optimal control and sub-optimal control, $\alpha = 0.12$. ——: $p(t)$ at optimal control. ——: $p(t)$ at sub-optimal control. ——: $\beta(t)$ at optimal control. ——: $\beta(t)$ at sub-optimal control.

$[t_3, t_5]$ denote the intervals with $p > 0$ and $p < 0$. Further, $[t_1, t_2]$ and $[t_3, t_4]$ indicate the subintervals with the valve closed corresponding to $\beta(t) = 0$, which causes the pressure to increase and decrease rapidly in these intervals. The valve is opened at the times t_2 and t_4 corresponding to $\beta(t) = 1$, which brings forward a temporarily decrease and increase of $p(t)$, as indicated by local extremes of the pressure.

At the optimal control, the length of the time interval with a closed valve varies somewhat due to the random sea-state. The idea of the considered sub-optimal control is to use a constant time interval with a closed valve of the length $\alpha T_p = t_2 - t_1 = t_4 - t_3$ at both positive and negative dynamic pressure. Then, the sub-optimal semi-active control of the valve can be written as

$$\begin{aligned} \beta(t) \;=\; & H\big(p(t)\big)H\big(t - t_1 - \alpha T_p\big) \\ & + H\big(-p(t)\big)\,H\big(t - t_3 - \alpha T_p\big) \end{aligned} \tag{31}$$

where $H(t)$ is the unit step function, defined as:

$$H(t) = \begin{cases} 1\,, & t \ge 0 \\ 0\,, & t < 0 \end{cases} \tag{32}$$

The optimal control value of α for a given sea-state is obtained by maximizing the absorbed energy of the sub-optimal controller in a given control interval relative to the absorbed energy at optimal control using the same sufficiently long realization of the surface elevation and the same wave load vector $\mathbf{f}_e(t)$. In Fig. 14, the performance of the sub-

1949-3029 (c) 2019 IEEE. Personal use is permitted, but republication/redistribution requires IEEE permission. See http://www.ieee.org/publications_standards/publications/rights/index.html for more information.

This article has been accepted for publication in a future issue of this journal, but has not been fully edited. Content may change prior to final publication. Citation information: DOI 10.1109/TSTE.2019.2923279, IEEE Transactions on Sustainable Energy

optimal controller has been indicated with a red signature, using the exact wave load vector and $\alpha = 0.12$.

The computational cost of the nonlinear programming calculation grows exponentially with the length of the control interval. For this reason the statistical stable optimal solution for α can hardly be achieved by merely using a single realization of the wave load process $\mathbf{f}_e(t)$. Instead a finite number N of independent realizations of the wave load vector processes of limited length is generated, each of which provides a sample of α based on nonlinear programming. Next, the final estimate of α is obtained by an ensemble average of these sample values. In this case, the calculation time merely grows linearly with N. Assuming that all involved stochastic processes are ergodic both of these approaches are equivalent.

With $\beta(t)$ given by (31), the state variables $\mathbf{u}(t)$ and $p(t)$ can be obtained by numerical time integration if the wave load vector $\mathbf{f}_e(t)$ can be estimated. $\mathbf{f}_e(t)$ depends on future surface elevations, which needs to be predicted at least one peak period T_p ahead, cf. the discussion related to Fig. 7. The prediction will be performed by a suitable Kalman-Bucy filter.

IV. Estimation of Wave Load Vector

At first a rational approximation to $S_{\eta\eta}(\omega)$ driven by unit intensity Gaussian white noise is devised, given as

$$S_{\eta\eta}(\omega) \simeq \frac{P(s)\,P(-s)}{Q(s)\,Q(-s)}\,\frac{1}{2\pi} \quad , \quad s = i\omega \tag{33}$$

Fig. 15 shows the rational approximation of order $(r, s) = (3, 6)$ to the double-side JONSWAP auto-spectral density function $S_{\eta\eta}(\omega)$ for the surface elevation given by (29).

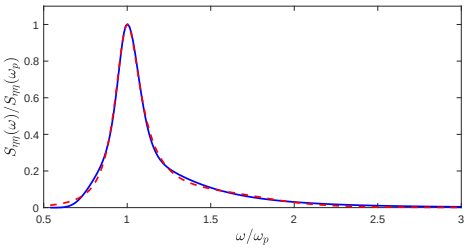

Fig. 15: Rational approximation to JONSWAP $S_{\eta\eta}(\omega)$ of order $(3, 6)$. ——: $S_{\eta\eta}(\omega)$. - - - : Rational approximation.

Then, the state equations for the surface elevation can be expressed as, [24]:

$$\left\{\begin{array}{l} \dfrac{d\mathbf{Y}(t)}{dt} = \mathbf{A}_c\mathbf{Y}(t) + \mathbf{b}_c\,w_1(t) \\ \eta(t) = \mathbf{p}_c\,\mathbf{Y}(t) + c\,w_2(t) \end{array}\right. \tag{34}$$

where $c\,w_2(t)$ is the measurement noise, c is a constant indicating the noise level. $w_1(t)$ and $w_2(t)$ are the unit intensity Gaussian white noises defined by the following mean value function and auto-covariance function:

$$\left.\begin{array}{l} E[w_\alpha(t)] = 0 \\ E[w_\alpha(t)\,w_\beta(t+\tau)] = \delta_{\alpha\beta}\,\delta(\tau) \end{array}\right\} \quad , \quad \alpha\,,\,\beta = 1, 2. \tag{35}$$

where $\delta(\cdot)$ is the Dirac function and $\delta_{\alpha\beta}$ is the Kronecker's delta. The column vectors $\mathbf{Y}(t)$, $\mathbf{b}_c$, the row vector $\mathbf{p}_c$ and the system matrix $\mathbf{A}_c$ has the similar expressions as shown in Eqs. (22), (23) and (24). Hence the optimal Kalman-Bucy observer equation reads, [25]:

$$\frac{d\hat{\mathbf{Y}}(t)}{dt} = \mathbf{A}_c\hat{\mathbf{Y}}(t) + \mathbf{K}(t)\big(\eta(t) - \mathbf{p}_c\,\hat{\mathbf{Y}}(t)\big) \tag{36}$$

where $\hat{\mathbf{Y}}(t)$ is the estimated state vector. $\mathbf{K}(t)$ indicates the time dependent Kalman gain vector, expressed as:

$$\mathbf{K}(t) = \mathbf{P}(t)\mathbf{p}_c^T\,\frac{1}{c^2} \tag{37}$$

where $\mathbf{P}(t) = E[\mathbf{e}(t)\,\mathbf{e}(t)^T]$ is the covariance matrix of the error vector $\mathbf{e}(t) = \mathbf{Y}(t) - \hat{\mathbf{Y}}(t)$. The stationary value of $\mathbf{P}(t)$ as $t \to \infty$ is given by the following algebraic Riccati equation, [25]:

$$\mathbf{A}_c\,\mathbf{P} + \mathbf{P}\,\mathbf{A}_c^T - \mathbf{P}\mathbf{p}_c^T\,\frac{1}{c^2}\mathbf{p}_c\,\mathbf{P} + \mathbf{b}_c\,\mathbf{b}_c^T = \mathbf{0} \tag{38}$$

Then, the prediction equation is expressed as:

$$\frac{d\bar{\mathbf{Y}}(\tau)}{d\tau} = \mathbf{A}_c\,\bar{\mathbf{Y}}(\tau) \quad , \quad \tau \in [t, t + T_\eta] \tag{39}$$

where $\bar{\mathbf{Y}}(\tau)$ is the predicted state vector at the time τ, t the present time and T_η the prediction horizon.

Hence, the predicted surface elevation $\bar{\eta}(\tau)$ can be obtained:

$$\bar{\eta}(\tau) = \mathbf{p}_c\,\bar{\mathbf{Y}}(\tau) = \mathbf{p}_c\,e^{\mathbf{A}_c\,(\tau - t)}\,\hat{\mathbf{Y}}(t)\ ,\ \tau \in [t, t + T_f] \tag{40}$$

where $e^{\mathbf{A}_c\,\tau}$ signifies the exponential matrix function, and the initial vector $\bar{\mathbf{Y}}(t)$ is the smoothed estimate from (36).

V. Numerical Example

The following parameter values have been applied. As seen, the stiffness of the mooring system is ignored in the example.

TABLE I: Heave absorber and wave excitation parameters

Parameter	Value	Unit	Parameter	Value	Unit
a	2.00	m	m_1	8.3695×10^5	kg
b	5.00	m	$m_{11}(\infty)$	3.4515×10^5	kg
h	100.00	m	$m_{12} = m_{21}$	2.5644×10^4	kg
D	5.00	m	$m_{22}(\infty)$	0.3736×10^5	kg
D_1	10.00	m	H_s	2.50	m
D_2	10.00	m	T_p	6.77	s
ρ_0	1.225	$\mathrm{kg/m^3}$	γ	3.3	
ρ_w	1025	$\mathrm{kg/m^3}$	k	1×10^{-3}	m·s
p_0	101325	Pa	c	0.1	m
k_m	0	N/m			

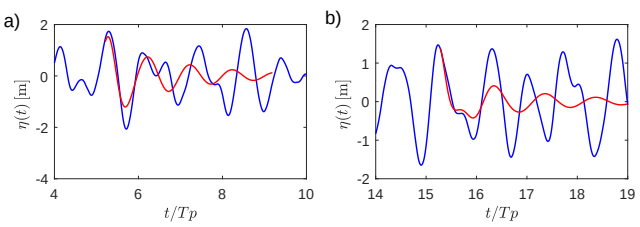

Fig. 16: Prediction of $\bar{\eta}(t)$ of the surface elevation for different start times with noise level $c = 0.1\mathrm{m}$. $T_p = 6.77\mathrm{s}$, $\mathrm{H_s} = 2.5\mathrm{m}$, $\gamma = 3.3$. a) Start at $\tau = 5.2T_p$. b) Start at $\tau = 15.3T_p$. ——: Reference $\eta(t)$. ——: Predicted $\bar{\eta}(\tau)$.

1949-3029 (c) 2019 IEEE. Personal use is permitted, but republication/redistribution requires IEEE permission. See http://www.ieee.org/publications_standards/publications/rights/index.html for more information.

This article has been accepted for publication in a future issue of this journal, but has not been fully edited. Content may change prior to final publication. Citation information: DOI 10.1109/TSTE.2019.2923279, IEEE Transactions on Sustainable Energy

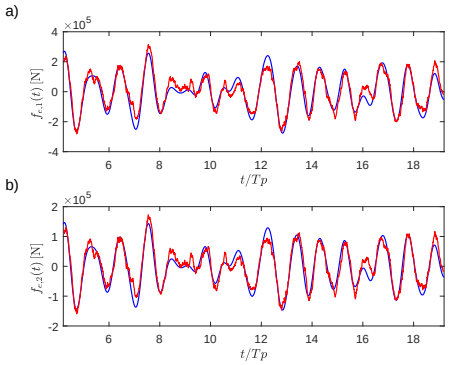

Fig. 17: Estimate of wave load vector $\mathbf{f}_e(\tau)$ with noise level $c = 0.1\text{m}$ corresponding to continuous predicted surface elevations. a) Predicted wave load component $\bar{f}_{e,1}(\tau)$. b) Predicted wave load component $\bar{f}_{e,2}(\tau)$. ——: Reference $\mathbf{f}_e(t)$. ——: Estimated $\bar{\mathbf{f}}_e(\tau)$.

Fig. 16 shows the prediction of surface elevation compared to the reference time series given in Fig. 11. As seen, predictions beyond T_p becomes inaccurate.

Fig. 17 shows the related estimate of $\mathbf{f}_e(t)$. At each instant of time, the surface elevation has been predicted one wave peak period ahead. Then, in combination with the previous surface elevations of the time series, the estimate of $\mathbf{f}_e(t)$ has been obtained from (6). At practical applications of the control, the previous surface elevations are assumed to be available from continuous measurements. The deviation from the reference value is a consequence of the prediction error of the surface elevation and the measurement noise.

Next, based on the average of $N = 4$ independent realizations of the length $30T_p$ of the surface elevation for a given sea state, the optimal value of the control parameter α can be obtained by maximizing the absorbed energy as indicated by (17). The red curve in Fig. 20 shows the variation of the absorbed energy as a function of α, where the exact wave loads related to the time series of surface elevations have been applied. As seen, a maximum is obtained approximately at $\alpha = 0.12$, where the reduction compared with the optimal absorbed energy as indicated by the blue line is 5.95%. For $\alpha = 0$, corresponding to a constantly open valve, the reduction is 10.24%.

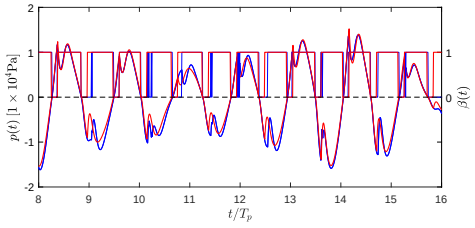

Fig. 18: $p(t)$ and $\beta(t)$ at optimal control and sub-optimal control with estimated wave load vector, $\alpha = 0.12$. ——: $p(t)$ at optimal control. ——: $p(t)$ at sub-optimal control. ——: $\beta(t)$ at optimal control. ——: $\beta(t)$ at sub-optimal control.

Fig. 18 shows the comparison of the variation of $\beta(t)$ and $p(t)$ at optimal control and sub-optimal control with $\alpha = 0.12$ and the estimated $\mathbf{f}_e(t)$ indicated in Fig. 17. A small deviation is obtained between the pressure variation at optimal and suggested sub-optimal control.

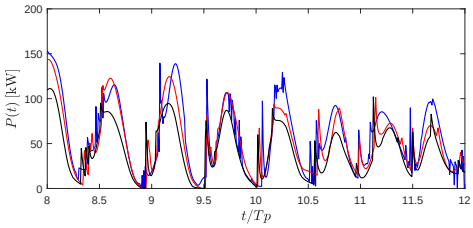

Fig. 19: Instantaneous Power take-off for different controls. ——: Power take-off at optimal control. ——: Power take-off at sub-optimal control with exact wave loads, $\alpha = 0.12$. ——: Power take-off at sub-optimal control with estimated wave loads, $\alpha = 0.12$.

Fig. 19 shows the instantaneous power take-off for the optimal control, the sub-optimal control using exact wave loads, and the sub-optimal control with estimated wave loads. All curves have been obtained as the average of the results from the previously mentioned $N = 4$ independent realizations of the surface elevation. $\alpha = 0.12$ is used in both sub-optimal controls.

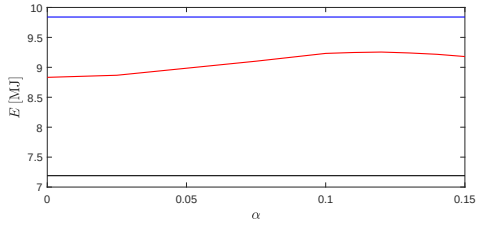

Fig. 20: Absorbed energy of sub-optimal controller as a function of α.

The black line in Fig. 20 indicates the average absorbed energy of the sub-optimal controller with $\alpha = 0.12$ and estimated wave loads for the $N = 4$ considered realizations of the surface elevation. The performance of the controller is 26.93% below that of the optimal controller and 22.31% below that of the sub-optimal controller with $\alpha = 0.12$ and exact wave loads. Hence, the primary reason of the indicated reduction is related to the estimation error of the wave loads.

VI. Conclusion

The paper focuses on the optimal control of a floating oscillating water column wave energy point absorber for power take-off. The piston model has been used for simulating the motion of the water column, and a linear model was used for the mass flow to the turbine. A semi-active control algorithm was suggested, where the opening and closing of the valve between the pressure chamber and the turbine is given as a fixed fraction of the peak period of the considered sea-state. The optimal value of the said fraction was determined by comparison to the optimal solution obtained by nonlinear programming. The devised control strategy relies on the estimation of the wave loads on the float and the wave column, which were obtained by a Kalman-Bucy filter prediction of the future sea surface elevation. The performance of the devised controller has been compared to that of the optimal control obtained by nonlinear programming. It is demonstrated that

1949-3029 (c) 2019 IEEE. Personal use is permitted, but republication/redistribution requires IEEE permission. See http://www.ieee.org/publications_standards/publications/rights/index.html for more information.

This article has been accepted for publication in a future issue of this journal, but has not been fully edited. Content may change prior to final publication. Citation information: DOI 10.1109/TSTE.2019.2923279, IEEE Transactions on Sustainable Energy

the reduced performance primarily is related to the errors of the wave load estimation.

ACKNOWLEDGMENT

The authors gratefully acknowledge the financial support from project 675659-ICONN-H2020-MSCA-ITN-2015.

REFERENCES

[1] A.F. Falcao, J.C. Henriques, "Oscillating-water-column wave energy converters and air turbines: a review", *Renew. Energy*, vol. 85, pp. 1391-1424, 2015.
[2] J. Falnes,"Wave-energy conversion through relative motion between two single-mode oscillating bodies", *Journal of Offshore Mechanics and Arctic Engineering*, vol. 121, no. 1, pp. 32-38, 1999.
[3] R.E. Hoskin, B.M. Count, N.K. Nichols, D.A.C. Nicol, " Phase control for the oscillating water column.", *In Hydrodynamics of Ocean Wave-Energy Utilization*, pp. 257-268, 1986. Springer, Berlin, Heidelberg.
[4] R.V. Gamkrelidze, L.S. Pontrjagin, V.G.E. Boltjanskij, "The mathematical theory of optimal processes", Macmillan Company, 1964.
[5] W.A. Gruver, E. Sachs, "Algorithmic Methods in Optimal Control", Pitman, 1980.
[6] J.C.C. Henriques, A.F.O. Falcao, R.P.F. Gomes, L.M.C. Gato, "Latching control of an OWC spar-buoy wave energy converter in regular waves", *In ASME 2012 31st International Conference on Ocean, Offshore and Arctic Engineering*, pp. 641-650, 2012, American Society of Mechanical Engineers.
[7] A. Brito-Melo, L.M.C. Gato, A.J.N.A Sarmento, "Analysis of Wells turbine design parameters by numerical simulation of the OWC performance", *Ocean Engineering*, vol. 29, no. 12, pp. 1463-1477, 2002.
[8] A.J. Garrido, I. Garrido, M. Amundarain, M. Alberdi, M. De la Sen, "Sliding-mode control of wave power generation plants", *IEEE Transactions on Industry Applications*, vol. 48, no. 6, pp. 2372-2381, 2012.
[9] M. Alberdi, et al., "Complementary control of oscillating water column-based wave energy conversion plants to improve the instantaneous power output", *IEEE Transactions on Energy Conversion*, vol. 26, no. 4, pp. 1021-1032, 2011.
[10] A. El Marjani, F.C. Ruiz, M.A. Rodriguez, M.P. Santos, "Numerical modelling in wave energy conversion Systems", *Energy*, vol. 33, no. 8, pp. 1246-1253, 2008.
[11] D.V. Evans, "The oscillating water column wave-energy device", *IMA Journal of Applied Mathematics*, vol. 22, no. 4, pp. 423-433, 1978.
[12] D.V. Evans, " Wave-power absorption by systems of oscillating surface pressure distributions", *Journal of Fluid Mechanics*, vol. 114, pp. 481-499, 1982.
[13] R.W. Robinson," The effects of geometric-wavefield interactions on the performance of oscillating water column wave energy converters". Queen's University of Belfast, 1982.
[14] J. Falnes,"Ocean waves and oscillating systems: linear interactions including wave-energy extraction", Cambridge university press, 2002.
[15] C.H. Lee, J.N. Newman, WAMIT User manual. WAMIT, Inc, 2016
[16] A.J. Sarmento and A.D.O. Falcäo, " Wave generation by an oscillating surface-pressure and its application in wave-energy extraction " , *Journal of Fluid Mechanics*, 150, pp. 467-485, 1985.
[17] A.F.D.O. Falcao, L.C. Vieira, P.A.P. Justino, and J.M.C.S. Andre, "By-pass air-valve control of an OWC wave power plant.", *Journal of Offshore Mechanics and Arctic Engineering*, vol. 125, no. 3, pp. 205210, 2003.
[18] A.J. Garrido, et al., "Mathematical modeling of oscillating water columns wave-structure interaction in ocean energy plants.", *Mathematical Problems in Engineering*, 2015.
[19] J. Lekube, A.J. Garrido, I. Garrido, "Rotational Speed Optimization in Oscillating Water Column Wave Power Plants Based on Maximum Power Point Tracking," in IEEE Transactions on Automation Science and Engineering, vol. 14, no. 2, pp. 681-691, 2017.
[20] A.J.N.A. Sarmento, L.M.C. Gato, A.D.O. Falco, "Turbine-controlled wave energy absorption by oscillating water column devices", *Ocean engineering*, vol. 17, no. 5, pp. 481-497, 1990.
[21] T. Perez, T.I. Fossen, "A matlab toolbox for parametric identification of radiation-force models of ships and offshore structures".
[22] K., Hasselmann, T.P. Barnett, E. Bouws, et al., "Measurements of wind wave growth and swell decay during the Joint North Sea Project (JONSWAP)", Deutches Hydrographisches Institut, 1973.
[23] T. Sun, S.R.K. Nielsen, "Stochastic optimal control of a heave point wave energy converter based on a modified LQG approach", *Ocean Engineering*, 154, 357-366, 2018.
[24] S.R.K. Nielsen, Z. Zhang, "Stochastic Dynamics". Aarhus University Press, 2017.
[25] L. Meirovitch, "Dynamics and Control of Structures", John Wiley & Sons, 1990.

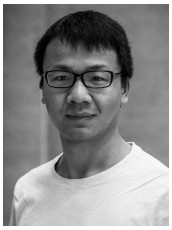

Tao Sun is a currently PhD student at the Department of Civil Engineering, Aalborg University, Denmark. His major research area is vibration control of offshore structures.

Søren R.K. Nielsen is a professor at the Department of Civil Engineering, Aalborg University, Denmark. His research areas include stochastic and nonlinear dynamics, elastodynamics, structural reliability theory and vibration control.

1949-3029 (c) 2019 IEEE. Personal use is permitted, but republication/redistribution requires IEEE permission. See http://www.ieee.org/publications_standards/publications/rights/index.html for more information.